DOI:
10.1021/acs.jmedchem.0c00494

Document Version
Peer reviewed version

Imaging biotin trafficking in vivo with positron emission tomography

Salvatore Bongarzone*, Teresa Sementa, Joel Dunn, Jayanta Bordoloi, Kavitha Sunassee, Philip Blower and Antony Gee*

ABSTRACT: The water-soluble vitamin biotin is essential for cellular growth, development and well-being but its absorption, distribution, metabolism, and excretion are poorly understood. This paper describes the radiolabelling of biotin with the positron emission tomography (PET) radionuclide carbon-11 ([^{11}C]biotin) to enable the quantitative study of biotin trafficking *in vivo*. We show that intravenously administered [^{11}C]biotin is quickly distributed to liver, kidneys, retina, heart and brain in rodents - consistent with the known expression of the biotin transporter – and a surprising accumulation in brown adipose tissue (BAT). Orally administered [^{11}C]biotin was rapidly absorbed in the small intestine and swiftly distributed to these same organs. Pre-administration of non-radioactive biotin inhibited organ-uptake and increased excretion. [^{11}C]Biotin PET imaging therefore provides a dynamic *in vivo* map of transporter-mediated biotin trafficking in healthy rodents. This technique will enable exploration of biotin trafficking in humans and its use as a research tool for diagnostic imaging in obesity/diabetes, bacterial infection and cancer.

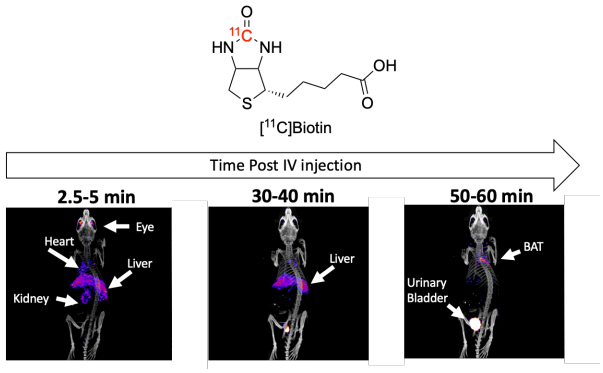

■ INTRODUCTION

Biotin (vitamin B7) is a cofactor for five carboxylases involved in fatty acid biosynthesis, gluconeogenesis and catabolism of amino acids and fatty acids.[1] Catalysis by mammalian biotin-dependent carboxylases drives incorporation of a single CO_2 carbon unit into molecules such as pyruvate, β-methylcrotonyl-CoA, propionyl-CoA and acetyl-CoA. Four out of five carboxylases are located in the mitochondria, and accordingly, biotin deficiencies result in abnormal mitochondrial structure and function.[2] Biotin is taken up by cells *via* the sodium-dependent vitamin transporter (SMVT), expressed in the cytoplasm and mitochondrial membranes. SMVT is present in the gastrointestinal tract, liver, kidneys, retina, heart, brain, and skin.[3-11] Cancer cells, including leukemia, ovarian, colon, mastocytoma, lung, renal, and breast cancer cell lines, exhibit elevated SMVT expression and enhanced biotin uptake capability to sustain their rapid cell growth and enhanced proliferation.[12]

To date, biotin uptake *via* SMVT has been studied with tritium (^{3}H) and carbon-14 (^{14}C) radiolabelled biotin in cell-based assays and in laboratory animal studies.[13-19] However *in vivo* investigations using these radiotracers are limited in scope because of low stability of [^{3}H]biotin in *vivo* (the tritium atoms at positions 8 and 9 in the valeric acid side chain are removed *in vivo via* β-oxidation - confounding the tissue distribution analysis).[18] For example, about half of the radioactivity associated with the administered dose of [^{3}H]biotin was excreted in 24 hours as [^{3}H]acetate/[^{3}H]H_2O in the urine of pigs.[18] Additional limitations include the need for *post-mortem* analysis to determine the radiotracer tissue distribution, precluding human translational studies,[18, 20] and the long radioactive half-life of ^{3}H (12.5 years) and ^{14}C (5,700 years) - impeding their use due to the associated risks of long-term radioactivity exposure. In this work we aimed to overcome these limitations by radiolabelling biotin with a positron emitting radionuclide that can be used for *in vivo* imaging, in both animals and humans, by positron emission tomography (PET).

Biotin has already been radiolabelled using PET and single-photon emission computed tomography (SPECT) radionuclides such as ^{64}Cu, ^{18}F, ^{111}In, ^{125}I, ^{131}I, ^{68}Ga and ^{99m}Tc,[21-28] and conjugated with fluorophores for optical imaging.[29-31] However, these "biotin-inspired" imaging probes have been developed *via* the conjugation of the carboxylic group of biotin to chelators or linkers bearing a radionuclide or a fluorophore. These radiotracers have been used in preclinical and clinical settings to detect *Escherichia coli* and *Staphylococcus aureus* infection which express biotin transporters (BirB and BioY, respectively)[32-36] and tumour antigens by exploiting the strong interaction ($K_d \approx 10^{-15}$ M) between radiolabelled biotin and pre-accumulated antibody-avidin conjugates (pre-targeting approach).[24, 28, 37, 38] The biotin-conjugated fluorescent probes have been used in preclinical and fluorescence images showed accumulation in tumour tissue of murine xenograft tumour models.[29-31] However, these tracers are biotin conjugates with grossly modified structures and their *in vivo* profile is not consistent with

literature reports of authentic biotin biodistribution and transporter expression.[26, 27] Indeed, changes to the carboxylic acid function (esterification, amidation, decarboxylation) or heterocyclic moiety (sulfoxidation and elimination of the ureido carbonyl group) prevent their bio-recognition by biotin transporters.[39-41]

Our aim is to characterize the whole-body pharmacokinetics and tissue-distribution of biotin *in vivo*. To achieve this, we have developed a method to produce biotin autologously radiolabelled with short-lived positron-emitting radionuclide carbon-11 ([^{11}C]biotin). Carbon-11 labelling of biotin does not alter its chemical structure or biological properties. Moreover, it allows straightforward translation from preclinical to clinical research, without toxicological assessment, and reduces risks associated with radioactive waste management and patient radiation exposure due to the short half-life of ^{11}C (half-life = 20.4 minutes).

■ RESULTS AND DISCUSSION

Radiosynthesis of [^{11}C]biotin. In developing our carbon-11 labelling strategy, we initially considered a previously described [^{14}C]biotin labelling procedure using [^{14}C]phosgene ([^{14}C]$COCl_2$) and diamino biotin *via* a multistep process to introduce carbon-11 in the urea position.[42] Although [^{11}C]$COCl_2$ has previously been obtained from cyclotron-produced carbon-11 carbon dioxide ([^{11}C]CO_2), it is impractical, requiring long synthesis times (15-25 minutes) using dedicated infrastructure, only available in a few radiochemistry laboratories world-wide, limiting its use.[43]

Inspired by new ^{11}C-urea labelling methods using the primary cyclotron-produced [^{11}C]CO_2 synthon,[44-46] we conceived a novel route to produce [^{11}C]biotin starting from diamino biotin. Applying this quick and efficient chemistry to the ^{11}C-labelling of biotin at the urea carbon atom, [^{11}C]biotin was synthesised via a simple two-step, one-pot reaction in a fully automated system (Figures 1 and S1). In the first step, cyclotron-produced [^{11}C]CO_2 was bubbled into a reaction vial containing diamino biotin (**1**) and 1,8-diazabicyclo[5.4.0]undec-7-ene (DBU) dissolved in acetonitrile (MeCN) at 0 °C. Then a solution of Mitsunobu reagents [di-*tert*-butyl azodicarboxylate (DBAD) and tributylphosphine (PBu_3)] was added to the reaction vial and the reaction mixture heated at 100 °C for 5 minutes. The reaction was subsequently cooled and quenched with a PBS solution. [^{11}C]Biotin was purified using semipreparative high-performance liquid chromatography (HPLC) and the formulated solution used for *in vitro* and *in vivo* experiments (Figure S2). Total synthesis time including HPLC purification was 32 ± 1 minutes from end of [^{11}C]CO_2 delivery.

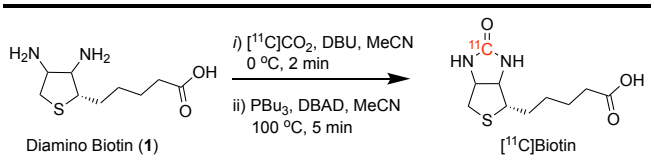

Scheme 1. Radiolabeling of [^{11}C]biotin.

Reagents and conditions: i) diamino biotin (1 equiv., 22.9 mmol), [^{11}C]CO_2, DBU (4.5 equiv.), MeCN (300 mL), 2 minutes at 0 °C; ii) PBu_3 (6 equiv., 137.3 mmol), DBAD (6 equiv., 137.3 mmol), MeCN (200 mL), 5 minutes at 100 °C.

The amount of [^{11}C]biotin obtained was 352 ± 38 MBq in 4-5 mL phosphate-buffered saline (PBS) with 2.5% ethanol in injectable solution starting from 5.9 ± 0.3 GBq of cyclotron produced [^{11}C]CO_2 with an isolated radiochemical yield (RCY) of 19 ± 2%, radiochemical purity (RCP) >99% and molar activity (A_m) of 7 ± 1 GBq/μmol at end of [^{11}C]CO_2 delivery (Table S1).

In vitro studies

Incubation of [^{11}C]biotin with streptavidin for 5 minutes at 25 °C showed that 95 ± 1% of the radioactivity is in the form of [^{11}C]biotin-streptavidin complex (see Supporting Information for assay details and Figure S3).

Preclinical studies of [^{11}C]biotin

Results of [^{11}C]biotin injected in mice

To examine [^{11}C]biotin trafficking *in vivo*, [^{11}C]biotin was administered intravenously (IV) in healthy anaesthetized mice placed in a high-resolution microPET scanner. Sixteen mice were divided into three groups: group A1 (female, vehicle IV injection 10 minutes before [^{11}C]biotin IV injection, n=6, Figure S4), group A2 (male, vehicle IV injection 10 minutes before [^{11}C]biotin IV injection , n=5) and group A3 (female, biotin 5 mg/Kg IV injection 10 minutes before [^{11}C]biotin IV injection, n=5). Dynamic PET image data were acquired for 60 minutes.

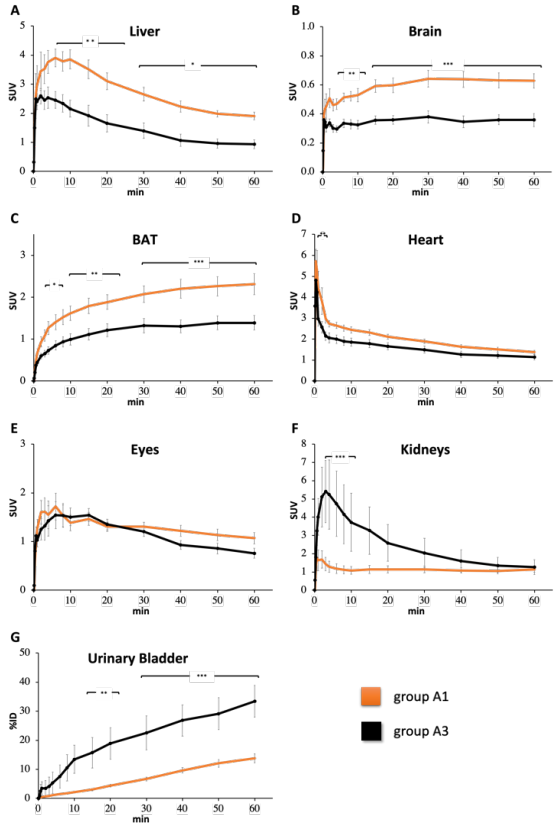

Figure 1. Time-SUV profile (0-60 minutes) of liver (A), brain (B), BAT (C), heart (D), eyes (E), kidneys (F) in NBA (orange line, group A1) and biotin-challenged (black line, group A3) mice receiving [^{11}C]biotin IV. The radioactivity of urinary bladder (G) is expressed as %ID. Note that the y-scale (SUV) varies between the different tissues.

In the no-biotin-added (NBA) group (group A1), PET imaging demonstrated [^{11}C]biotin uptake in liver, heart, brain, eyes, kidneys and interscapular BAT (Figures 1 and 2). The presence

of SMVT transporter in the liver,[3, 6] heart,[7, 8] brain,[5, 10] eyes[4] and kidney[11] provides a rationale for the observed [^{11}C]biotin distribution *in vivo*. To date, no reports have established the presence of SMVT transporter in BAT. Further studies (e.g. immunohistochemistry) are needed to confirm the expression of biotin transporters in BAT. However, uptake in BAT is consistent with prior knowledge that fatty acid synthesis, glucose metabolism and lipolysis require biotin-dependent enzymes, and that biotin-deficient rats have decreased adipose biotin-dependent mitochondrial enzyme function.[7, 8] Biotin is also known to be essential for the differentiation of preadipocytes into brown adipocytes.[47-49] [^{18}F]Fluorodeoxyglucose ([^{18}F]FDG) and fatty-acid radiotracers (e.g. [^{11}C]acetate, [^{123}I]beta-methyl-iodophenyl-pentadecanoic acid) have recently revealed that BAT serves as a metabolic sink for glucose and fatty acids.[50-52]

To further examine the relation between *in vivo* [^{11}C]biotin distribution and SMVT expression, male mice (group A2) and female mice challenged with biotin (group A3, Figure S4) were imaged.

To examine the uptake transporter at blood-tissue interfaces, we determined the radioactivity concentrations in blood of groups A1-A3. The image-derived blood curve was generated by placing a region of interest into the left ventricle of the heart.[53] Radioactivity concentrations measured in the last PET time frame (50-60 min post administration) showed good correlation ($r = 0.910$, $P < 0.0001$) with radioactivity concentration (%ID/g) in venous blood collected at the end of the PET scan measured in a γ counter (**Figure S6**). Liver-to-blood, kidney-to-blood, BAT-to-blood and brain-to-blood area under the curve (AUC) radioactivity ratios ($K_{p,tissue,\ AUC}$) were calculated (eq. 1). The 'integration plot' analysis[53-56] was used to calculate the liver uptake ($CL_{uptake,liver}$), kidney uptake ($CL_{uptake,kidney}$), BAT uptake ($CL_{uptake,BAT}$), brain uptake ($CL_{uptake,brain}$) and intrinsic urinary excretion ($CL_{int,urine}$) clearances which represent the uptake in the liver/kindey/BAT/brain and intrinsic efflux activity across the corticomedullary region of the kidney, respectively.

Blood radioactivity concentrations were lower ($p < 0.05$) for groups A2 and A3 than for the control group. $AUC_{liver\ 0–60\ min}$ was higher in group A2 and lower in groups A3 than control mice (group A1). The liver-to-blood AUC ratio ($K_{p,liver,AUC}$) and $CL_{uptake,liver}$ was higher in group A2 than in control group mice. No statistically significant difference was observed for the $K_{p,liver,AUC}$ and $CL_{uptake,liver}$ of group A3 *versus* control mice. The $K_{p,kidney,AUC}$ was not different between groups A1 and A2, however the $CL_{uptake,kidney}$ in groups A2 was significantly higher than in control mice (**Table 1**). Both $K_{p,kidney,AUC}$ and $CL_{uptake,kidney}$ (**Table 1**) values were significantly higher in groups A3 than in control mice. Although $AUC_{BAT,\ 0–60\ min}$ and $AUC_{brain,\ 0–60\ min}$ were lower in groups A2 and A3 than in control mice, $K_{p,BAT,AUC}$, $CL_{uptake,BAT}$, $K_{p,brain,AUC}$, $CL_{uptake,brain}$ of group A1 *versus* groups A2 or A3 were not statistically different (**Tables 1**).

Next, we used graphical methods [57-59] to establish the binding kinetics of [^{11}C]biotin in liver, kidney, brain and BAT. We estimated the volume of distribution (V_T, Table 1) for reversible binding and net uptake rate constant (K_i) for irreversible binding using the Logan and Patlak graphical methods, respectively.[57-59] Logan plots for liver and kidneys are shown in **Figure S7**, the plot linearity indicating a reversible tracer behaviour for these tissues in all groups.

Table 1 Pharmacokinetic Parameters of [^{11}C]biotin in groups A1-A3

	Group A1 Control group	Group A2	Group A3
Body weight †	17 ± 1	24 ± 1*	17 ± 1
$AUC_{blood,\ 0–60\ min}$ (SUV· min) †	135.8 ± 10.1	96.0 ± 8.8*	97.2 ± 9.4*
$AUC_{liver,\ 0–60\ min}$ (SUV · min) †	160.5 ± 12.1	220.8 ± 6.6**	86.1± 11.0**
$AUC_{BAT,\ 0–60\ min}$ (SUV · min) †	116.2 ± 10.1	63.1 ± 5.1**	69.5 ± 6.9**
$AUC_{Kindey,\ 0–60\ min}$ (SUV ·min)	77.2 ± 9.0	98.9 ± 13.8	172.3 ± 41.1
$AUC_{brain,\ 0–60\ min}$ (SUV · min) †	35.9 ± 2.6	26.3 ±2.1**	20.5 ± 1.4***
$K_{p,liver,\ AUC,\ 60\ min}$ (mL/g of tissue) †	1.22 ± 0.17	2.35 ± 0.15***	0.88 ± 0.06
$K_{p,kidney,\ AUC,\ 60\ min}$ (mL/g of tissue) †	0.59 ± 0.08	1.02 ±0.05	1.74 ± 0.39*
$K_{p,BAT,\ AUC,\ 60\ min}$ (mL/g of tissue)	0.87 ± 0.08	0.66 ± 0.03	0.73 ± 0.08
$K_{p,brain,AUC,\ 60\ min}$ (mL/g of tissue)	0.27 ± 0.03	0.28 ± 0.02	0.21 ± 0.01
$V_{T,liver}$† ***mL/g of tissue***	1.27 ± 0.16	2.54 ±0.18***	0.91 ±0.06
$V_{T,kidney}$† ***mL/g of tissue***	0.58 ±0.08	1.00 ± 0.04**	1.99 ±0.49*
$K_{i,\ BAT}$	0.021 ± 0.004	0.051 ± 0.012	0.027 ± 0.007
$K_{i,brain}$	0.005 ± 0.001	0.015 ± 0.004	0.004 ± 0.001
$CL_{uptake,liver}$ **(mL/min/g tissue)** †	0.37 ± 0.07	1.35 ± 0.34**	0.37 ± 0.12
$CL_{uptake,Kidney}$ † **(*mL/min/g tissue*)**	0.28 ± 0.09	2.02 ± 0.54*	1.37 ± 0.28*
$CL_{uptake,BAT}$ **(*mL/min/g tissue*)**	0.13 ± 0.03	0.24 ± 0.07	0.12 ± 0.03
$CL_{uptake,brain}$ **(*mL/min/g tissue*)**	0.05 ± 0.01	0.18 ± 0.07	0.05 ± 0.01
$X_{urine,0–60\ min}$ (% dose) †	13.8 ± 1.5	30.4 ± 3.3**	34.7 ± 5.5*
$Cl_{renal\text{-}blood}$ (ml/min/Kg)	1.7 ± 0.4	16.6 ± 5.6	7.2 ± 2.2
$CL_{int,urine}$† ***ml/min/Kg***	1.9 ± 0.2	3.8 ± 0.14***	2.8 ± 1.0

† One way ANOVA $p<0.05$. Body weight, AUC, K_p, X, and K_i were analysed using a one-way ANOVA. For this analysis $p<0.05$ was considered significant and post-hoc t-tests were used to explore these differences between pairs of groups. Levene's test was used to test for homogeneity of variances between the 3 groups and where this was significant ($p<0.05$), Welch's test for equality of means was used in place of ANOVA and t-tests assuming unequal variances were used to explore the group differences where appropriate. Groups A2 and A3 were compared to group A1 and indicated with (*) for $p < 0.05$, (**) for $p < 0.01$, and (***) for $p < 0.001$.

Logan plots for BAT and brain (**figure S7**) were non-linear indicating non-reversible tracer behaviour in these tissues. This is confirmed by Patlak analysis which shows good fits for BAT and brain indicating that [^{11}C]biotin is irreversibly trapped in these tissues for the duration of the scan (**Figure S8**). Notably, the K_i values are similar (**Table 1**) however flux of [^{11}C]biotin from blood to BAT and brain is the product of K_i and the concentration of free biotin in the blood. Although we did not directly measure the concentration of biotin in the blood it is reasonable to assume the group A3 had a much higher blood biotin concentration than group A1 and therefore, with equal K_i, flux of biotin trapped in BAT and brain was proportionally higher. As with many PET quantitative techniques, graphical methods

can be sensitive to ROI placement. Further studies are required to elucidate the biological mechanisms which determine biotin uptake.

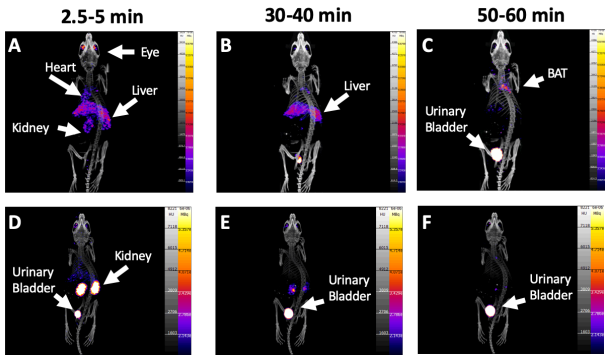

Figure 2. Maximum intensity projections of PET images from NBA (upper row, group A1) and biotin-challenged (lower row, group A3) mice at 2.5-5 minutes (A and D), 30-40 minutes (B and E) and 50–60 minutes (C and F) post [^{11}C]biotin IV injection. Tracer uptake is reduced in biotin-challenged mice in BAT, liver, heart and eyes. PET images are displayed according to the intensity scale for tracer activity, from white (highest), through red (intermediate) to purple (lowest).

A significant increase of [^{11}C]biotin excretion was observed in the both male (group A2) and the biotin-challenged female groups (group A3) compared to the NBA group (group A1) (Figure 1). A remarkable increase in [^{11}C]biotin uptake was observed in the kidneys groups A2 and A3 mice *versus* control group (group A1) in the first 10 minutes (**Figure 1**). From 10 to 60 minutes the radioactivity in the kidney in both groups decreased with a concomitant increase in the urinary bladder. The urinary excretion was 2.2 and 2.5 times higher in A2 and A3 groups, respectively, than that in the control group. Gender has a significant impact in renal clearance with increased $CL_{renal,blood}$ and $CL_{int,urine}$ higher in male *versus* female mice (**Table 1**). Regarding the increase of [^{11}C]biotin-urinary excretion in biotin-challenged mice, we postulate that this may be a consequence of saturation of SMVT expressed in proximal tubular epithelial cells.[11, 40, 60, 61] Saturation would preclude biotin reabsorption and facilitate the clearance of [^{11}C]biotin, consistent with our observations of radioactivity excretion *via* the kidney and urinary bladder (Figure 2D-F).

These studies demonstrated that the fraction of [^{11}C]biotin excreted is dose dependant. This implies that the homeostasis of vitamins is fine-tuned by the body and the administration of high concentrations of biotin increases its excretion (total biotin administered in biotin-challenged mice was ~40 times higher than NBA mice). In line with these results, high excretion rates have been observed in biotin-challenged rats after intraperitoneal (IP) injection of [^{14}C]biotin at doses of 0.005, 0.04, and 10 mg/Kg where 47%, 83% and >90% of the administered radioactivity, respectively, was found in the urine within 12 hours.[17]

Ex vivo biodistribution post-[^{11}C]biotin injection. The *ex vivo* biodistribution analysis of groups A1-A3 at 70 minutes post-[^{11}C]biotin injection showed radioligand uptake >10% ID/g in liver, kidneys and heart (**Figure S9**). Liver/blood ratio uptake (**Table S3**) was higher in male than female mice. This *ex vivo* biodistribution result was in agreement with the *in vivo* uptake parameter ($K_{p,liver,AUC}$) obtained from PET imaging at 60 minutes post-[^{11}C]biotin administration. Biodistribution analysis of biotin-challenged mice (group A3) showed a lower liver/blood ratio than control group (group A1, **Table S3**).

Radiometabolite analysis post-[^{11}C]biotin injection. Radiometabolite analysis by TLC-autoradiography was performed by following the protocol developed by McCormick D. B. *et al.* which has been validated to separate the main [^{14}C]biotin radiometabolites in rat urine.[17] In our experiments (see Supporting Information for assay details), only intact [^{11}C]biotin was detected in the urine of NBA and biotin-challenged groups, consistent with previous studies of [^{14}C]biotin metabolomics in biotin-challenged rats (10 mg/kg, 12 hours post IP injection) and NBA pigs (24 ng/kg, 24 hours post IV injection).[17, 18] These studies also reported that the administration of low doses of [^{14}C]biotin (10 ng/kg, IP injection) in rats showed two radiometabolites: [^{14}C]bisnorbiotin (29%) and [^{14}C]biotin sulfoxide (10%) at the later timepoint of 3 hours post-administration.[19] It is important to note that bisnorbiotin and biotin sulfoxide are not substrates for SMVT.[40] The absence of [^{11}C]biotin radiometabolites in our experiments might be due to species differences (mice *versus* rats), concentration of biotin in the formulation (2 µg/kg *versus* 10 ng/kg), the early urine sampling timepoint (70 minutes *versus* 3 hours) or the radiotracer route administration (IV *versus* IP injection). A limitation of our preclinical rodent study is that we were unable to perform plasma metabolite analysis during the PET image acquisition.

[^{11}C]biotin orally administered in mice. Humans and other mammals must obtain biotin *via* the gastrointestinal absorption.[9] Thus, to examine biotin gastrointestinal absorption and body circulation *in vivo*, [^{11}C]biotin was orally administered in mice. Ten anaesthetized female mice were divided into two groups: group B1 (orogastric (OG) administration of vehicle 10 minutes before [^{11}C]biotin OG administration, n=5, Figure S4) and group B2 (biotin OG administration, 5 mg/Kg, 10 minutes before [^{11}C]biotin OG administration, n=5).

To establish the relative contribution of intestinal SMVT to biotin OG absorption, small-animal PET imaging studies were conducted in isoflurane-anaesthetized mice for 120 minutes post-administration of [^{11}C]biotin. Demonstrating differential oral absorption between these two groups is highly valuable as it provides new insight into the role of SMVT expressed in the intestinal epithelium in absorption of dietary biotin and delivery to the circulation. Thus, we investigated the gastric emptying, intestinal absorption and tissue distribution of OG delivered [^{11}C]biotin (Figure 3A-C).

Gastric emptying by 2 hours was ~75% (Figures 3A and S10A) with no differences between groups. A complete gastric emptying was not observed as the anaesthesia reduces the gastrointestinal peristaltic movement.[62] Indeed, dynamic PET studies showed that gastric emptying was a major factor in limiting complete [^{11}C]biotin absorption because once delivered into the intestine, [^{11}C]biotin was rapidly absorbed in the duodenum (no radioactivity was observed in the large intestine, Figure 4 and S10B). Almost all [^{11}C]biotin delivered to the small intestine (92%) was absorbed after 20 min in the NBA group (group B1), in contrast with a much lower [^{11}C]biotin absorption in biotin-challenged mice (56% in group B2) (Figures 3B and 4). Biotin-challenged mice absorbed almost all [^{11}C]biotin delivered to the

small intestine (80%) at 80 minutes post radiotracer administration.

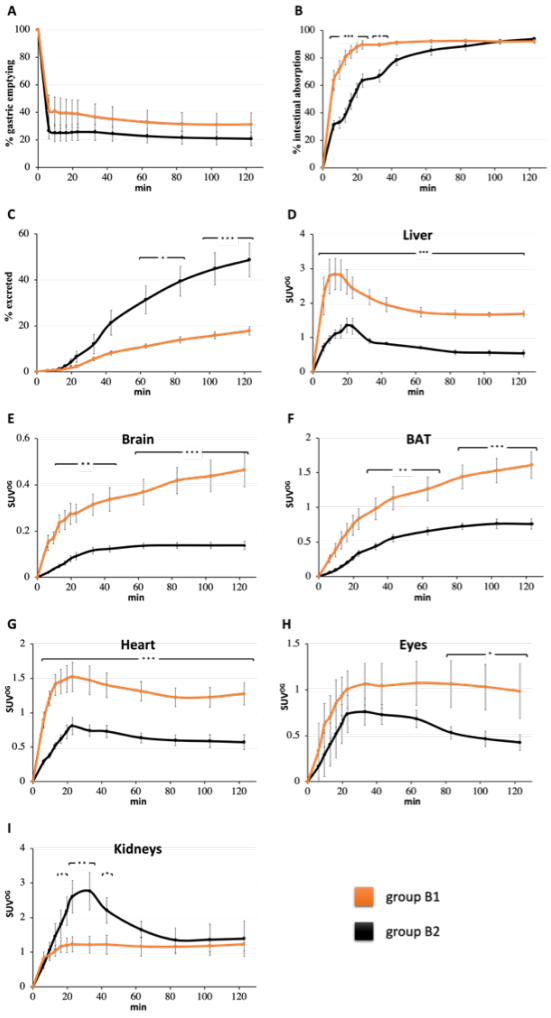

Figure 3. Time (0-120 minutes)-% gastric emptying profile (A), time-% intestinal absorption profile (B), time-% excretion profile (C) and time-SUV^{OG} profile for liver (D), brain (E), BAT (F), heart (G), eyes (H), kidneys (I) in NBA (orange line, group B1) and biotin-challenged (black line, group B2) mice receiving [^{11}C]biotin OG. Data are the mean ± SEM. Note that the y-scale (SUV^{OG}) varies between the different tissues.

The [^{11}C]biotin absorbed by the intestine entered the systemic circulation and was distributed throughout the body (Figure 4A-C) in liver, heart, eyes, brain and interscapular BAT. The organ distribution of [^{11}C]biotin administered orally matches with that observed after IV administration. Compared with the NBA group (group B1), biotin-challenged mice (group B2) showed a 2- to 4-fold decrease in [^{11}C]biotin uptake in all SMVT-expressing organs (liver, brain and BAT, heart, eyes) from 10 to 120 minutes post-administration and more than 2-fold higher concentration in the kidneys at 30 minutes (Figure 4D-F). NBA and biotin-challenged mice excreted 18% and 49% of the total administered radioactivity within 120 minutes, respectively (Figure 3C), suggesting a saturation effect of the biotin challenge which results in faster elimination of bulk biotin through the kidneys to the urinary bladder.

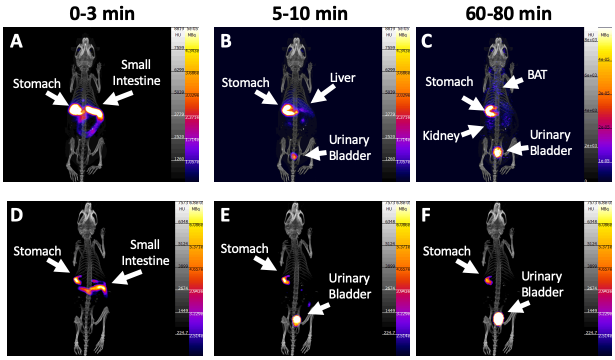

Figure 4. Maximum intensity projections of PET images from NBA (upper row, group B1) and biotin-challenged (lower row, group B1) mice receiving [^{11}C]biotin OG at 0-3 minutes (A and D), 5-10 minutes (B and E) and 60–80 minutes (C and F) after start of the PET imaging study. PET images are displayed according to the intensity scale for tracer activity, from white (highest), through red (intermediate) to purple (lowest). Stomach, intestine, urinary bladder, liver, kidney and BAT are indicated where visible.

The potential use of [^{11}C]biotin as a research tool for diagnostic imaging in obesity/diabetes, bacterial infection and cancer

Based on these results, [^{11}C]biotin might be a valuable tool for imaging BAT function in humans, particularly in light of clinical studies suggesting an association between decreased BAT function and obesity and diabetes.[63, 64] In translational anti-obesity and anti-diabetes research, pharmacological activation of BAT thermogenesis is a potential strategy for increasing energy expenditure. The gold standard PET radiotracer for the *in vivo* visualization of BAT is [^{18}F]FDG, but glucose uptake might not reflect BAT thermogenesis as fatty acids obtained from intracellular triglyceride lipolysis, not glucose, are the primary substrate for activated BAT.[65, 66] Therefore, the involvement of biotin-dependent enzymes in fatty acid metabolism suggest that BAT uptake of [^{11}C]biotin might reflect BAT thermogenesis activity. The validation of [^{11}C]biotin as tool to monitor BAT thermogenesis activity will require further studies in rodents under cold exposure or pharmacological interventions (e.g. norepinephrine or propranolol).

Other potential applications of [^{11}C]biotin include the diagnosis and localisation of bacterial infection and cancer *via* a direct-labelling or pre-targeting strategy. Firstly, the uptake of biotin by *E. Coli* is highly efficient, but the modification of the carboxylic acid moiety of biotin reduces the affinity to bacterial transporters 50-fold.[67] [^{11}C]Biotin, possessing a free carboxylic acid, might have similar or better prospects for imaging bacterial infection compared with the "biotin-inspired" radiotracers in which the carboxylic group is modified. Secondly, various aggressive cancer cell lines such as ovarian, leukemia, mastocytoma, colon, breast renal, and lung cancer cell lines overexpress SMVT.[12] In anti-cancer drug development, biotin-drug conjugation enhances tumour delivery of drugs and anti-cancer effects.[68] The use of [^{11}C]biotin in cancer might be useful for cancer diagnosis/management and understanding the role of SMVT in tumorigenesis.

Alongside the potential of [^{11}C]biotin as an imaging biomarker in pathological conditions, its clinical translation will allow the study of whole-body biotin trafficking in healthy humans receiving an adequate intake level (30 mg/day) and supplemented (10 mg/day) daily doses of biotin to form the basis of rational dosing regimen for this essential micronutrient. High biotin intake (300 mg/day) has shown positive effects in reducing disability progression in multiple sclerosis patients by activating myelin synthesis and enhancing energy production in demyelinated nerves.[69, 70] A multi-centre randomized double blind placebo controlled study evaluating 300 mg/day of biotin in 642 multiple sclerosis patients is underway (clinical trial: NCT02936037). In our work, [^{11}C]biotin administered by OG mimics the main route of intake of biotin in humans and other mammals. Intestinal absorption of [^{11}C]biotin in mouse is rapid, and virtually complete within minutes. Our OG studies indicate that [^{11}C]biotin can be used to investigate further factors such as age, the effect of vitamin supplements, drugs, food, and pathological conditions of the gastrointestinal tract that may affect biotin absorption and trafficking. Gastrointestinal absorption in humans might be difficult to predict from the results of these preclinical animal studies due to species differences and the administration of anaesthesia which lowers gastrointestinal peristaltic movements. However, this preclinical PET imaging study provides the fundamental methodology to investigate the gastrointestinal absorption and whole-body biotin trafficking in humans.

■ CONCLUSIONS

In this report, we have demonstrated for the first time the feasibility of using a short-lived radioactive carbon-11 isotopologue of biotin to non-invasively study authentic biotin trafficking *in vivo* using micro-PET imaging. This was made possible by the first radiosynthesis of [^{11}C]biotin, achieved using cyclotron-produced [^{11}C]CO_2 to radiolabel a commercially available precursor using a novel radiochemical reaction in a fully automated radiolabelling procedure. Here, we advance our understanding of the *in vivo* biodistribution and kinetics of [^{11}C]biotin and the molecular mechanisms of biotin absorption in mice by studying different routes of administration (IV *versus* OG), gender differences (male *versus* female) and the effect of biotin challenge (NBA *versus* BC). IV or OG administration of [^{11}C]biotin to female mice revealed accumulation in SMVT-expressing organs such as heart, eyes, brain, liver and BAT.

Interestingly, the *in vivo* distribution of "biotin-inspired" imaging agents are not consistent with the known expression of SMVT transporters, confirming that the use of authentic [^{11}C]biotin is crucial to elucidate the true behaviour of biotin-dependent mechanisms *in vitro* and *in vivo*. In conclusion, the current work lays the foundation for mapping SMVT in disease models, the understanding of biotin's role in BAT thermogenesis and the prospect of a new translational tool to study biotin absorption and trafficking in humans in health and disease.

■ EXPERIMENTAL SECTION

Production of [^{11}C]biotin

The automated radiosynthesis of [^{11}C]biotin was performed on an Eckert & Ziegler (E&Z) Modular Lab system with the configuration (Figure S1). Prior to production, an automated "flow test" sequence in the Eckert & Ziegler (E&Z) software was performed by applying helium pressure into the system to check that the flow of gases was not obstructed, and the system was gas tight. The preparation for each run also included an automated "conditioning" sequence. [^{11}C]Biotin was prepared according to the following stepwise procedure.

[^{11}C]CO_2 was produced in a cyclotron by the ^{14}N(p,α)^{11}C nuclear reaction in a carbon-11 gas target filled with N_2 containing 0.5% O_2. The standard parameters for production were 15 μA for 8 minutes, with an estimated yield at the EOB of approximately 7-8 GBq of [^{11}C]CO_2. Cyclotron-produced [^{11}C]CO_2 was bubbled in a stream of helium gas directly into a solution (vial A) containing diamino biotin (5 mg, 22.9 μmol, 1 equiv.), DBU (4.5 equiv.) in MeCN (300 μL) at 0 °C for 1.75 minutes. At the end of [^{11}C]CO_2 delivery, DBAD (6 equiv.) and PBu_3 (6 equiv.) dissolved in 200 μL MeCN (vial C) were transferred to the reaction vial under a positive pressure of helium. The vial heated at 100 °C for 5 minutes (Figure S1) with helium flow at 60 mL/min and the solvent distilled in Vial B kept at -20 °C. Then the Vial A was cooled at 25 °C and PBS solution from Vial D was transferred with helium (100 mL/min) to Vial A. The crude mixture was transferred to an HPLC injection loop through a vent filter. The reaction purified by semipreparative HPLC using a mobile phase composed by 2.5% ethanol in 10 mM PBS buffer solution (pH = 7.4). The mixture was transferred to an HPLC loop (2 mL) for subsequent semipreparative HPLC purification using a reversed-phase HPLC column (Discovery® C18 HPLC Column, 5 μm particle size, 25 cm length, 10 mm internal diameter) equipped with a radioactivity detector (radio-RP-HPLC) and eluted with a mobile phase composed of 2.5% ethanol in PBS, pH = 7.4 at a flow rate of 4 mL/min (retention time: 12.6 min). The [^{11}C]biotin peak was collected in a vented sterile vial through a 0.22 μm filter. Analytical HPLC analysis for the quality control (QC) of the final tracer product was carried out on an HPLC analytical C18 column (Discovery® C18 HPLC Column, 5 μm particle size, 15 cm length, 4.6 mm internal diameter, Figure S2A-C).

Quality control (QC) of [^{11}C]biotin

Analytical HPLC analysis for the QC of the final tracer product was carried out on an Agilent 1200 HPLC system equipped with a UV detector (λ=210 nm) and a β+-flow detector coupled in series. The samples were injected on to an analytical Discovery C18 column (Discovery® C18 HPLC Column, 5 μm particle size, 15 cm length, 4.6 mm internal diameter), which was eluted with a mobile phase of 2.5% ethanol in 10 mM PBS. The column flow rate is 1 mL/min and was kept at 25 °C (Figure S2A). The typical retention of biotin is in between 4:08 minutes for the UV absorbance (the radioactivity detector is 15 seconds at 1 mL/min further downstream from the UV detector, Figure S2B) and the radiochemical purity (RCP) was >99%. A linear regression is determined for UV absorbance peak areas of the standards. This constitutes the calibration curve. Then the UV peak area of the [^{11}C]biotin formulation is fit on the calibration curve to determine the biotin concentration in the formulation and A_m.

Biodistribution and PET Imaging Studies with [^{11}C]biotin *in vivo.*

In vivo studies were carried out in male and female mice (Balb/C, Charles River UK Ltd). All animal studies were carried out in accordance with the UK Home Office Animals (Scientific Procedures) Act 1986. Experiments complied with UK Research Councils' and Medical Research Charities' guidelines on responsibility in the use of animals in bioscience research, under UK Home Office project and personal licenses. The reporting of this study complied with the Animal Research: Reporting in vivo experiments (ARRIVE) guidelines (https://www.nc3rs.org.uk/arrive-guidelines). In order to assess and compare the *in vivo* distributions of [^{11}C]biotin, the mice were divided into five groups. Each group of mice was allocated to: 1) the NBA IV female group, 2) the NBA IV male group, 3) the biotin-challenged IV female group, 4) the NBA OG female group and 5) the biotin-challenged OG female. Mice of age 56-66 days were selected because they have an ideal size to perform a total body imaging in our small-animal PET. PET/CT scans were taken once on each mouse using one administration route (Figure S4). A limitation of the studies in this work is the challenge to carry out dynamic microPET experiments on fully

conscious rodents because of ethical and practical concerns so the mice were taken under anaesthesia for the entire protocol study.

PET/CT Imaging in Mice.

Dynamic PET scans (1:5 coincidence mode; 5-ns coincidence time window) were performed on a nanoScan PET/CT 8W scanner (Mediso Ltd., Budapest, Hungary) over 60 (groups A1-A3) or 120 minutes (groups B1-B2) followed by CT (180 projections, 55 kVp X-ray source, 600-ms exposure time, 1:4 binning and semi-circular acquisition) using their proprietary acquisition software (Nucline 1.07). Ten minutes before the *in vivo* protocol was scheduled to start, mice were anaesthetised in a heated induction box by inhalation of 2% isoflurane in 100% oxygen.

For IV injection protocol, 30 µL of vehicle composed of 2.5% ethanol in 10 mM phosphate buffer solution (PBS, pH 7.4, NBA group) or biotin (3.3 mg/mL, 2.5% ethanol in PBS, biotin-challenged group) was administered IV. After 10 minutes, [^{11}C]biotin (146 ± 8 µL, 4.6 ± 0.8 MBq, Table S2) was administered IV (Figure S4A). The IV administrations were carried out via the tail vein cannula in mice positioned on a heated PET-CT small animal holder. There was no lag between the injection of [^{11}C]biotin and start of the PET acquisition. The syringe radioactivity was measured before and after administration to calculate the injected dose (ID).

For OG administration protocol, 30 µL of vehicle (2.5% ethanol in PBS, NBA group) or biotin (3.3 mg/mL, 2.5% ethanol in PBS, biotin-challenged group) was administered by OG. After 10 minutes, [^{11}C]biotin (175 ± 6 µL, 6.1 ± 1.1 MBq) was administered by OG (Figure S4B). For dynamic microPET studies, anaesthetised animals were placed on the PET-CT holder immediately after OG of [^{11}C]biotin and a 2 hour PET scan started; a delay of approximately 2.5-3 minutes between tracer delivery due to the time taken to administered [^{11}C]biotin by OG and position the animal in the scanner. PET scan initiation has been taken when representing the data in Figures 3 and 4. The syringe radioactivity was measured before and after administration to calculate the administered dose.

After completion of the PET data acquisition, computed tomography (CT) scans were performed to provide anatomical information. CT images were acquired over 7 minutes. After the PET/CT scans, animals were culled (70- and 130-minutes post radiotracer IV injection and OG administration, respectively).

Analysis of PET Data

Whole-body Tera-Tomo (Mediso) 3-dimensional reconstruction was performed (400–600-keV energy window, 1–3 coincidence mode, 4 iterations and 6 subsets) using an isotropic voxel size of 0.4 mm^3. Images were corrected for attenuation, scatter, and decay. The acquired data were binned into sixteen image frames (2 ×10, 2 × 20, 3 × 60, 3 × 120, 2 × 300, and 4 × 600 seconds) for Figures 1 and 2 and twelve image frames (6 × 200 and 2 × 600 and 4 × 1200 seconds) for Figures 3 and 4. VivoQuant® software (Version 3.5, InviCRO Inc., http://www.vivoquant.com/) was used for image display and volume-of-interest (VOI) analysis. In each experiment, VOI for the whole mouse, liver, kidneys, brain, heart, BAT, and eyes were drawn manually. For animals receiving [^{11}C]biotin IV, SUV = [decay-corrected tissue radioactivity concentration (Bq/ml)/(injected dose (Bq)] × body weight (g).

The apparent tissue–to–blood area under the curve (AUC) ratio ($K_{p,liver,AUC}$, $K_{p,kidney,AUC}$, $K_{p,BAT,AUC}$, $K_{p,brain,AUC}$) was calculated using the following equation:

$$K_{p,tissue,AUC} = \frac{AUC_{tissue,0-60}}{AUC_{blood,0-60}} \qquad \text{eq. 1}$$

where $AUC_{tissue,0–60\ min}$ represents the area under the tissue radioactivity concentration–time curve for the time period 0–60 min and $AUC_{blood,0–60\ min}$ represents the area under the blood radioactivity concentration–time curve for the time period 0–60 min.

The renal clearance ($CL_{renal,blood,0–60\ min}$) with respect to the blood radioactivity concentration was calculated using the following equations:

$$CL_{renal,;blood,0-60\ min} = \frac{X_{urine,0-60\ min}}{AUC_{blood,0-60min}} \qquad \text{eq. 2}$$

where $X_{urine,\ 0\text{-}60\ min}$ represents the amount of radioactivity secreted into the urine between 0 and 60 min.

For animals receiving [^{11}C]biotin by OG, SUV^{OG} = [decay-corrected tissue radioactivity concentration (Bq/ml)/ (administered dose minus radioactivity remaining in the stomach (Bq)] × body weight (g). In each experiment, volumes of interest (VOI) for the whole mouse, stomach, intestine, liver, kidneys, brain, heart, BAT, eyes and urinary bladder were drawn manually, and the radioactivity (Bq) in each VOI was estimated using VivoQuant software.

Gastric emptying and intestinal absorption in animals[71] receiving [^{11}C]biotin by OG were estimated by determining the radioactivity amount in stomach and small intestine, respectively, as a function of time. Gastric emptying was estimated from the ratio between the [^{11}C]biotin in the stomach and the amount in the whole-body. Intestinal absorption was estimated from the ratio between the amount of [^{11}C]biotin in the small intestine *versus* the amount in the whole-body minus the amounts remaining in the stomach.

Statistical analysis

Quantitative data were expressed as mean ± SEM. For Figures 1, 3, and S5, organ SUV at various time points of [^{11}C]biotin was compared between the groups using a repeated measures mixed-effect model with an auto-regressive covariance structure. Post-hoc analyses were corrected for multiple comparisons (IBM SPSS Statistics, Version 24.0). Differences at the 95% confidence level ($P < 0.05$) were considered significant. Data were indicated with (*) for $p < 0.05$, (**) for $p < 0.01$, and (***) for $p < 0.001$.

AUTHOR INFORMATION

Corresponding Author

*Corresponding Authors

Salvatore Bongarzone – *School of Biomedical Engineering & Imaging Sciences, King's College London, St Thomas' Hospital, London, SE1 7EH, United Kingdom. Email:Salvatore.bongarzone@kcl.ac.uk*
orcid.org/0000-0002-1309-3045

Antony Gee – *School of Biomedical Engineering & Imaging Sciences, King's College London, St Thomas' Hospital, London, SE1 7EH, United Kingdom. Email:antony.gee@kcl.ac.uk*
orcid.org/0000-0001-8389-9012

Authors

Teresa Sementa – *School of Biomedical Engineering & Imaging Sciences, King's College London, St Thomas' Hospital, London, SE1 7EH, United Kingdom.*

Joel Dunn – *School of Biomedical Engineering & Imaging Sciences, King's College London, St Thomas' Hospital, London, SE1 7EH, United Kingdom.*

Jayanta Bordoloi – *School of Biomedical Engineering & Imaging Sciences, King's College London, St Thomas' Hospital, London, SE1 7EH, United Kingdom.*

Kavitha Sunassee – *School of Biomedical Engineering & Imaging Sciences, King's College London, St Thomas' Hospital, London, SE1 7EH, United Kingdom.*

Philip Blower – *School of Biomedical Engineering & Imaging Sciences, King's College London, St Thomas' Hospital, London, SE1 7EH, United Kingdom.*

Author Contributions

S.B. and A.G. conceived the study. S.B. performed the radiosynthesis. K.S. and S.B. designed the preclinical protocol. J.B. and T.S. and S.B. performed preclinical experiments. T.S. and S.B. performed *ex vivo* biodistribution and metabolite analysis. S.B. and J.D. analysed the data. S.B., J.D., P. B., and A.G. interpreted the data and wrote the manuscript.

ACKNOWLEDGMENT

This work was supported by Medical Research Council [MRC, MR/K022733/1], European Commission FP7-PEOPLE-2012-ITN [316882, RADIOMI] and Wellcome Trust [WT 084052/Z/07/Z] and Wellcome/EPSRC Centre for Medical Engineering [WT 203148/Z/16/Z]. The research was supported by the National Institute for Health Research (NIHR) Biomedical Research Centre based at Guy's and St Thomas' NHS Foundation Trust and King's College London. The views expressed are those of the authors and not necessarily those of the NHS, the NIHR or the Department of Health.

ABBREVIATIONS USED

A_m, molar activity; AUC, area under the curve; BAT, brown adipose tissue; ^{11}C, carbon-11; ^{14}C, carbon-14; $CL_{int,urine}$, intrinsic urinary excretion clearance, CO_2, carbon dioxide; DBU, 8-diazabicyclo[5.4.0]undec-7-ene; DBAD, di-*tert*-butyl azodicarboxylate; [^{18}F]FDG, [^{18}F]Fluorodeoxyglucose; ID, injected dose,; ^3H, tritium; HPLC, high-performance liquid chromatography; IV, intravenous; IP, intraperitoneal; $K_{p,tissue,\ AUC,}$ tissue-to-blood area under the curve (AUC) radioactivity ratio; MeCN, acetonitrile; NBA, no-biotin-added; OG, orogastric; PBS, phosphate-buffered saline; PET, positron emission tomography; PBu_3, tributylphosphine; QC, quality controll; RCP, radiochemical purity; SMVT, sodium-dependent vitamin transporter; SPECT, single-photon emission computed tomography; SUV, standardized uptake value; and TLC, thin layer chromatography.

ASSOCIATED CONTENT

Supporting Information

The Supporting Information is available free of charge on the ACS Publications website.

Preparation of the synthesis module, representative radio-HPLC traces, *in vitro* [^{11}C]biotin-streptavidin binding, Graphical Plots, Figure S1-S10 and Table S1-S3 (PDF)

Molecular formula strings (CSV)

REFERENCES

(1) Said, H. M. Biotin: biochemical, physiological and clinical aspects. *Subcell. Biochem.* **2012**, *56*, 1-19.

(2) Ochoa-Ruiz, E.; Diaz-Ruiz, R.; Hernandez-Vazquez Ade, J.; Ibarra-Gonzalez, I.; Ortiz-Plata, A.; Rembao, D.; Ortega-Cuellar, D.; Viollet, B.; Uribe-Carvajal, S.; Corella, J. A.; Velazquez-Arellano, A. Biotin deprivation impairs mitochondrial structure and function and has implications for inherited metabolic disorders. *Mol. Genet. Metab.* **2015**, *116*, 204-214.

(3) Balamurugan, K.; Ortiz, A.; Said, H. M. Biotin uptake by human intestinal and liver epithelial cells: role of the SMVT system. *Am. J. Physiol. Gastrointest. Liver Physiol.* **2003**, *285*, G73-77.

(4) Ohkura, Y.; Akanuma, S.; Tachikawa, M.; Hosoya, K. Blood-to-retina transport of biotin via Na+-dependent multivitamin transporter (SMVT) at the inner blood-retinal barrier. *Exp. Eye Res.* **2010**, *91*, 387-392.

(5) Uchida, Y.; Ito, K.; Ohtsuki, S.; Kubo, Y.; Suzuki, T.; Terasaki, T. Major involvement of Na(+)-dependent multivitamin transporter (SLC5A6/SMVT) in uptake of biotin and pantothenic acid by human brain capillary endothelial cells. *J. Neurochem.* **2015**, *134*, 97-112.

(6) Said, H. M.; McAlister-Henn, L.; Mohammadkhani, R.; Horne, D. W. Uptake of biotin by isolated rat liver mitochondria. *Am. J. Physiol.* **1992**, *263*, G81-86.

(7) Mallet, R. T.; Sun, J. Mitochondrial metabolism of pyruvate is required for its enhancement of cardiac function and energetics. *Cardiovasc. Res.* **1999**, *42*, 149-161.

(8) Velazquez-Arellano, A.; Hernandez-Esquivel Mde, L.; Sanchez, R. M.; Ortega-Cuellar, D.; Rodriguez-Fuentes, N.; Cano, S.; Leon-Del-Rio, A.; Carvajal, K. Functional and metabolic implications of biotin deficiency for the rat heart. *Mol. Genet. Metab.* **2008**, *95*, 213-219.

(9) Chatterjee, N. S.; Kumar, C. K.; Ortiz, A.; Rubin, S. A.; Said, H. M. Molecular mechanism of the intestinal biotin transport process. *Am. J. Physiol.* **1999**, *277*, C605-613.

(10) Park, S.; Sinko, P. J. The blood-brain barrier sodium-dependent multivitamin transporter: a molecular functional in vitro-in situ correlation. *Drug Metab. Dispos.* **2005**, *33*, 1547-1554.

(11) Podevin, R. A.; Barbarat, B. Biotin uptake mechanisms in brush-border and basolateral membrane vesicles isolated from rabbit kidney cortex. *Biochim. Biophys. Acta* **1986**, *856*, 471-481.

(12) Ren, W. X.; Han, J.; Uhm, S.; Jang, Y. J.; Kang, C.; Kim, J. H.; Kim, J. S. Recent development of biotin conjugation in biological imaging, sensing, and target delivery. *Chem. Commun. (Camb)* **2015**, *51*, 10403-10418.

(13) Dakshinamurti, K.; Mistry, S. P. Tissue and intracellular distribution of biotin-C-1400H in rats and chicks. *J. Biol. Chem.* **1963**, *238*, 294-296.

(14) Kang, Y. S.; Saito, Y.; Pardridge, W. M. Pharmacokinetics of [3H]biotin bound to different avidin analogues. *J. Drug Target* **1995**, *3*, 159-165.

(15) Robinson, B. H.; Oei, J.; Saunders, M.; Gravel, R. [3H]Biotin-labeled proteins in cultured human skin fibroblasts from patients with pyruvate carboxylase deficiency. *J. Biol. Chem.* **1983**, *258*, 6660-6664.

(16) Wang, K. S.; Kearns, G. L.; Mock, D. M. The clearance and metabolism of biotin administered intravenously to pigs in tracer and physiologic amounts is much more rapid than previously appreciated. *J. Nutr.* **2001**, *131*, 1271-1278.

(17) Lee, H. M.; Wright, L. D.; McCormick, D. B. Metabolism of carbonyl-labeled 14 C-biotin in the rat. *J. Nutr.* **1972**, *102*, 1453-1463.

(18) Mock, D. M.; Wang, K. S.; Kearns, G. L. The pig is an appropriate model for human biotin catabolism as judged by the urinary metabolite profile of radioisotope-labeled biotin. *J. Nutr.* **1997**, *127*, 365-369.

(19) Wang, K. S.; Patel, A.; Mock, D. M. The metabolite profile of radioisotope-labeled biotin in rats indicates that rat biotin metabolism is similar to that in humans. *J. Nutr.* **1996**, *126*, 1852-1857.

(20) Fraenkel-Conrat, J.; Fraenkel-Conrat, H. Metabolic fate of biotin and of avidin-biotin complex upon parenteral administration. *Biochim. Biophys. Acta* **1952**, *8*, 66-70.

(21) Rusckowski, M.; Fogarasi, M.; Virzi, F.; Hnatowich, D. J. Influence of endogenous biotin on the biodistribution of labelled biotin derivatives in mice. *Nucl. Med. Commun.* **1995**, *16*, 38-46.

(22) Claesener, M.; Breyholz, H. J.; Hermann, S.; Faust, A.; Wagner, S.; Schober, O.; Schafers, M.; Kopka, K. Efficient synthesis of a fluorine-18 labeled biotin derivative. *Nucl. Med. Biol.* **2012**, *39*, 1189-1194.

(23) Shoup, T. M.; Fischman, A. J.; Jaywook, S.; Babich, J. W.; Strauss, H. W.; Elmaleh, D. R. Synthesis of fluorine-18-labeled biotin derivatives: biodistribution and infection localization. *J. Nucl. Med.* **1994**, *35*, 1685-1690.

(24) Kudo, T.; Ueda, M.; Konishi, H.; Kawashima, H.; Kuge, Y.; Mukai, T.; Miyano, A.; Tanaka, S.; Kizaka-Kondoh, S.; Hiraoka, M.; Saji, H. PET imaging of hypoxia-inducible factor-1-active tumor cells with pretargeted oxygen-dependent degradable streptavidin and a novel 18F-labeled biotin derivative. *Mol. Imaging Biol.* **2011**, *13*, 1003-1010.

(25) Lewis, M. R.; Wang, M.; Axworthy, D. B.; Theodore, L. J.; Mallet, R. W.; Fritzberg, A. R.; Welch, M. J.; Anderson, C. J. In vivo evaluation of pretargeted 64Cu for tumor imaging and therapy. *J. Nucl. Med.* **2003**, *44*, 1284-1292.

(26) Hnatowich, D. J.; Virzi, F.; Rusckowski, M. Investigations of avidin and biotin for imaging applications. *J. Nucl. Med.* **1987**, *28*, 1294-1302.
(27) Foulon, C. F.; Alston, K. L.; Zalutsky, M. R. Synthesis and preliminary biological evaluation of (3-iodobenzoyl)norbiotinamide and ((5-iodo-3-pyridinyl)carbonyl)norbiotinamide: two radioiodinated biotin conjugates with improved stability. *Bioconjug. Chem.* **1997**, *8*, 179-186.
(28) Prakash, S.; Hazari, P. P.; Meena, V. K.; Jaswal, A.; Khurana, H.; Kukreti, S.; Mishra, A. K. Biotinidase resistant 68gallium-radioligand based on biotin/avidin interaction for pretargeting: synthesis and preclinical evaluation. *Bioconjug. Chem.* **2016**, *27*, 2780-2790.
(29) Li, K.; Dong, W.; Liu, Q.; Lv, G.; Xie, M.; Sun, X.; Qiu, L.; Lin, J. A biotin receptor-targeted silicon(IV) phthalocyanine for in vivo tumor imaging and photodynamic therapy. *J. Photochem. Photobiol. B* **2019**, *190*, 1-7.
(30) Guo, R.; Huang, F.; Zhang, B.; Yan, Y.; Che, J.; Jin, Y.; Zhuang, Y.; Dong, R.; Li, Y.; Tan, B.; Song, R.; Hu, Y.; Dong, X.; Li, X.; Lin, N. GSH activated niotin-tagged near-infrared probe for efficient cancer imaging. *Theranostics* **2019**, *9*, 3515-3525.
(31) Bhuniya, S.; Maiti, S.; Kim, E. J.; Lee, H.; Sessler, J. L.; Hong, K. S.; Kim, J. S. An activatable theranostic for targeted cancer therapy and imaging. *Angew. Chem. Int. Ed. Engl.* **2014**, *53*, 4469-4474.
(32) Erba, P. A.; Cataldi, A. G.; Tascini, C.; Leonildi, A.; Manfredi, C.; Mariani, G.; Lazzeri, E. 111In-DTPA-Biotin uptake by Staphylococcus aureus. *Nucl. Med. Commun.* **2010**, *31*, 994-997.
(33) Lazzeri, E.; Erba, P.; Perri, M.; Tascini, C.; Doria, R.; Giorgetti, J.; Mariani, G. Scintigraphic imaging of vertebral osteomyelitis with 111In-biotin. *Spine* **2008**, *33*, E198-204.
(34) Rusckowski, M.; Paganelli, G.; Hnatowich, D. J.; Magnani, P.; Virzi, F.; Fogarasi, M.; DiLeo, C.; Sudati, F.; Fazio, F. Imaging osteomyelitis with streptavidin and indium-111-labeled biotin. *J. Nucl. Med.* **1996**, *37*, 1655-1662.
(35) Lazzeri, E.; Manca, M.; Molea, N.; Marchetti, S.; Consoli, V.; Bodei, L.; Bianchi, R.; Chinol, M.; Paganelli, G.; Mariani, G. Clinical validation of the avidin/indium-111 biotin approach for imaging infection/inflammation in orthopaedic patients. *Eur. J. Nucl. Med.* **1999**, *26*, 606-614.
(36) Lazzeri, E.; Pauwels, E. K.; Erba, P. A.; Volterrani, D.; Manca, M.; Bodei, L.; Trippi, D.; Bottoni, A.; Cristofani, R.; Consoli, V.; Palestro, C. J.; Mariani, G. Clinical feasibility of two-step streptavidin/111In-biotin scintigraphy in patients with suspected vertebral osteomyelitis. *Eur. J. Nucl. Med. Mol. Imaging* **2004**, *31*, 1505-1511.
(37) Paganelli, G.; Magnani, P.; Zito, F.; Villa, E.; Sudati, F.; Lopalco, L.; Rossetti, C.; Malcovati, M.; Chiolerio, F.; Seccamani, E.; Siccardi, A. G.; Fazio, F. Three-step monoclonal antibody tumor targeting in carcinoembryonic antigen-positive patients. *Cancer Res.* **1991**, *51*, 5960-5966.
(38) Kalofonos, H. P.; Rusckowski, M.; Siebecker, D. A.; Sivolapenko, G. B.; Snook, D.; Lavender, J. P.; Epenetos, A. A.; Hnatowich, D. J. Imaging of tumor in patients with indium-111-labeled biotin and streptavidin-conjugated antibodies: preliminary communication. *J. Nucl. Med.* **1990**, *31*, 1791-1796.
(39) Spencer, R. P.; Brody, K. R. Biotin transport by small intestine of rat, hamster, and other species. *Am. J. Physiol.* **1964**, *206*, 653-657.
(40) Baur, B.; Wick, H.; Baumgartner, E. R. Na(+)-dependent biotin transport into brush-border membrane vesicles from rat kidney. *Am. J. Physiol.* **1990**, *258*, F840-847.
(41) Ma, T. Y.; Dyer, D. L.; Said, H. M. Human intestinal cell line Caco-2: a useful model for studying cellular and molecular regulation of biotin uptake. *Biochim. Biophys. Acta* **1994**, *1189*, 81-88.
(42) Melville, D. B.; Pierce, J. G.; Partridge, C. W. The preparation of C14-labeled biotin and a study of its stability during carbon dioxide fixation. *J. Biol. Chem.* **1949**, *180*, 299-305.
(43) Rotstein, B. H.; Liang, S. H.; Placzek, M. S.; Hooker, J. M.; Gee, A. D.; Dolle, F.; Wilson, A. A.; Vasdev, N. 11C=O bonds made easily for positron emission tomography radiopharmaceuticals. *Chem. Soc. Rev.* **2016**, *45*, 4708-4726.
(44) Dheere, A. K. H.; Bongarzone, S.; Taddei, C.; Yan, R.; Gee, A. D. Synthesis of C-11-labelled symmetrical ureas via the rapid incorporation of [C-11]CO2 into aliphatic and aromatic amines. *Synlett* **2015**, *26*, 2257-2260.
(45) Dheere, A. K. H.; Yusuf, N.; Gee, A. Rapid and efficient synthesis of [C-11]ureas via the incorporation of [C-11]CO2 into aliphatic and aromatic amines. *Chem. Commun. (Camb)* **2013**, *49*, 8193-8195.
(46) Bongarzone, S.; Ferocino, A.; Gee, A. Expanding the scope of carbon-11 labelled ureas: a universal method to access short-lived click reagents for in vivo PET imaging. *J. Label. Compd. Radiopharm.* **2019**, *62*, S244-S245.
(47) Lee, P.; Swarbrick, M. M.; Zhao, J. T.; Ho, K. K. Inducible brown adipogenesis of supraclavicular fat in adult humans. *Endocrinology* **2011**, *152*, 3597-3602.
(48) Lee, M. J.; Fried, S. K. Optimal protocol for the differentiation and metabolic analysis of human adipose stromal cells. *Methods Enzymol.* **2014**, *538*, 49-65.
(49) Kuri-Harcuch, W.; Wise, L. S.; Green, H. Interruption of the adipose conversion of 3T3 cells by biotin deficiency: differentiation without triglyceride accumulation. *Cell* **1978**, *14*, 53-59.
(50) Saito, M.; Okamatsu-Ogura, Y.; Matsushita, M.; Watanabe, K.; Yoneshiro, T.; Nio-Kobayashi, J.; Iwanaga, T.; Miyagawa, M.; Kameya, T.; Nakada, K.; Kawai, Y.; Tsujisaki, M. High incidence of metabolically active brown adipose tissue in healthy adult humans: effects of cold exposure and adiposity. *Diabetes* **2009**, *58*, 1526-1531.
(51) Ouellet, V.; Labbe, S. M.; Blondin, D. P.; Phoenix, S.; Guerin, B.; Haman, F.; Turcotte, E. E.; Richard, D.; Carpentier, A. C. Brown adipose tissue oxidative metabolism contributes to energy expenditure during acute cold exposure in humans. *J. Clin. Invest.* **2012**, *122*, 545-552.
(52) Zhang, F.; Hao, G.; Shao, M.; Nham, K.; An, Y.; Wang, Q.; Zhu, Y.; Kusminski, C. M.; Hassan, G.; Gupta, R. K.; Zhai, Q.; Sun, X.; Scherer, P. E.; Oz, O. K. An adipose tissue atlas: an image-guided identification of human-like BAT and beige depots in rodents. *Cell Metab.* **2018**, *27*, 252-262 e253.
(53) Traxl, A.; Wanek, T.; Mairinger, S.; Stanek, J.; Filip, T.; Sauberer, M.; Muller, M.; Kuntner, C.; Langer, O. Breast cancer resistance protein and p-glycoprotein influence in vivo disposition of 11C-erlotinib. *J. Nucl. Med.* **2015**, *56*, 1930-1936.
(54) Shingaki, T.; Hume, W. E.; Takashima, T.; Katayama, Y.; Okauchi, T.; Hayashinaka, E.; Wada, Y.; Cui, Y.; Kusuhara, H.; Sugiyama, Y.; Watanabe, Y. Quantitative evaluation of mMate1 function based on minimally invasive measurement of tissue concentration using PET with [(11)C]metformin in mouse. *Pharm. Res.* **2015**, *32*, 2538-2547.
(55) Takano, A.; Kusuhara, H.; Suhara, T.; Ieiri, I.; Morimoto, T.; Lee, Y. J.; Maeda, J.; Ikoma, Y.; Ito, H.; Suzuki, K.; Sugiyama, Y. Evaluation of in vivo p-glycoprotein function at the blood-brain barrier among MDR1 gene polymorphisms by using 11C-verapamil. *J. Nucl. Med.* **2006**, *47*, 1427-1433.
(56) Takashima, T.; Wu, C.; Takashima-Hirano, M.; Katayama, Y.; Wada, Y.; Suzuki, M.; Kusuhara, H.; Sugiyama, Y.; Watanabe, Y. Evaluation of breast cancer resistance protein function in hepatobiliary and renal excretion using PET with 11C-SC-62807. *J. Nucl. Med.* **2013**, *54*, 267-276.
(57) Bertoldo, A.; Rizzo, G.; Veronese, M. Deriving physiological information from PET images: from SUV to compartmental modelling. *Clin. Transl. Imaging* **2014**, *2*, 239-251.
(58) Logan, J. Graphical analysis of PET data applied to reversible and irreversible tracers. *Nucl Med Biol* **2000**, *27*, 661-670.
(59) Zhou, Y.; Ye, W.; Brasic, J. R.; Wong, D. F. Multi-graphical analysis of dynamic PET. *Neuroimage* **2010**, *49*, 2947-2957.
(60) Balamurugan, K.; Vaziri, N. D.; Said, H. M. Biotin uptake by human proximal tubular epithelial cells: cellular and molecular aspects. *Am. J. Physiol. Renal. Physiol.* **2005**, *288*, F823-831.
(61) Spencer, P. D.; Roth, K. S. On the uptake of biotin by the rat renal tubule. *Biochem. Med. Metab. Biol.* **1988**, *40*, 95-100.
(62) Yamashita, S.; Takashima, T.; Kataoka, M.; Oh, H.; Sakuma, S.; Takahashi, M.; Suzuki, N.; Hayashinaka, E.; Wada, Y.; Cui, Y.; Watanabe, Y. PET imaging of the gastrointestinal absorption of orally administered drugs in conscious and anesthetized rats. *J. Nucl. Med.* **2011**, *52*, 249-256.
(63) van Marken Lichtenbelt, W. D.; Vanhommerig, J. W.; Smulders, N. M.; Drossaerts, J. M.; Kemerink, G. J.; Bouvy, N. D.; Schrauwen, P.; Teule, G. J. Cold-activated brown adipose tissue in healthy men. *N. Engl. J. Med.* **2009**, *360*, 1500-1508.
(64) Nedergaard, J.; Bengtsson, T.; Cannon, B. Unexpected evidence for active brown adipose tissue in adult humans. *Am. J. Physiol. Endocrinol. Metab.* **2007**, *293*, E444-452.
(65) Sampath, S. C.; Sampath, S. C.; Bredella, M. A.; Cypess, A. M.; Torriani, M. Imaging of brown adipose tissue: state of the art. *Radiology* **2016**, *280*, 4-19.
(66) Ong, F. J.; Ahmed, B. A.; Oreskovich, S. M.; Blondin, D. P.; Haq, T.; Konyer, N. B.; Noseworthy, M. D.; Haman, F.; Carpentier, A. C.; Morrison, K. M.; Steinberg, G. R. Recent advances in the detection of brown adipose tissue in adult humans: a review. *Clin. Sci. (Lond)* **2018**, *132*, 1039-1054.

(67) Piffeteau, A.; Zamboni, M.; Gaudry, M. Biotin transport by a biotin-deficient strain of Escherichia coli. *Biochim. Biophys. Acta* **1982**, *688*, 29-36.

(68) Maiti, S.; Paira, P. Biotin conjugated organic molecules and proteins for cancer therapy: a review. *Eur. J. Med. Chem.* **2018**, *145*, 206-223.

(69) Tourbah, A.; Lebrun-Frenay, C.; Edan, G.; Clanet, M.; Papeix, C.; Vukusic, S.; De Seze, J.; Debouverie, M.; Gout, O.; Clavelou, P.; Defer, G.; Laplaud, D. A.; Moreau, T.; Labauge, P.; Brochet, B.; Sedel, F.; Pelletier, J. MD1003 (high-dose biotin) for the treatment of progressive multiple sclerosis: a randomised, double-blind, placebo-controlled study. *Mult. Scler.* **2016**, *22*, 1719-1731.

(70) Sedel, F.; Bernard, D.; Mock, D. M.; Tourbah, A. Targeting demyelination and virtual hypoxia with high-dose biotin as a treatment for progressive multiple sclerosis. *Neuropharmacology* **2016**, *110*, 644-653.

(71) Sala-Rabanal, M.; Ghezzi, C.; Hirayama, B. A.; Kepe, V.; Liu, J.; Barrio, J. R.; Wright, E. M. Intestinal absorption of glucose in mice as determined by positron emission tomography. *J. Physiol.* **2018**, *596*, 2473-2489.